Non-equilibrium trajectory dynamics and the kinematics of gliding in a flying snake

Non-equilibrium trajectory dynamics and the kinematics of gliding in a flying snake

John J Socha[1,4]**, Kevin Miklasz**[2]**, Farid Jafari**[1] **and Pavlos P Vlachos**[3]

[1] Engineering Science and Mechanics, Virginia Tech, Blacksburg, VA 24061, USA
[2] Hopkins Marine Station, Stanford University, Pacific Grove, CA 93950, USA
[3] Department of Mechanical Engineering, Virginia Tech, Blacksburg, VA 24061, USA

E-mail: jjsocha@vt.edu

Abstract
Given sufficient space, it is possible for gliding animals to reach an equilibrium state with no net forces acting on the body. In contrast, every gliding trajectory must begin with a non-steady component, and the relative importance of this phase is not well understood. Of any terrestrial animal glider, snakes exhibit the greatest active movements, which may affect their trajectory dynamics. Our primary aim was to determine the characteristics of snake gliding during the transition to equilibrium, quantifying changes in velocity, acceleration, and body orientation in the late phase of a glide sequence. We launched 'flying' snakes (*Chrysopelea paradisi*) from a 15 m tower and recorded the mid-to-end portion of trajectories with four videocameras to reconstruct the snake's body position with mm to cm accuracy. Additionally, we developed a simple analytical model of gliding assuming only steady-state forces of lift, drag and weight acting on the body and used it to explore effects of wing loading, lift-to-drag ratio, and initial velocity on trajectory dynamics. Despite the vertical space provided to transition to steady-state gliding, snakes did not exhibit equilibrium gliding and in fact displayed a net positive acceleration in the vertical axis, an effect also predicted by the analytical model.

S Online supplementary data available from stacks.iop.org/BB/5/045002/mmedia

(Some figures in this article are in colour only in the electronic version)

1. Introduction

Gliding is the act of controlled descent in which gravitational potential energy is converted to useful aerodynamic work [1]. Although active flight is relatively uncommon among animals, occurring in only four groups (birds, bats, insects and extinct pterosaurs), many species have independently evolved the ability to glide, including mammals, frogs, lizards, snakes, ants, fish, and squid. Apart from the aquatic gliders, which become airborne by jumping out of water [2–4], all terrestrial gliders are exclusively arboreal [1], and most exhibit anatomical specializations that increase surface area for aerodynamic force production and control. Mammals, frogs, and lizards (genus *Draco*) stretch skin between bony struts to create membranous 'wings' that unfurl upon takeoff (see

figure 1). In mammals, the patagial skin runs between the front and rear legs and from the legs to body, creating rectangular wings with low aspect ratio [5–7]. Flying frogs have enlarged feet with skin webbing between the toes, providing four force-producing surfaces with large moment arms relative to the body (figures 1(*A*) and (*B*)) [8, 9]. *Draco* lizards use long, mobile ribs connected by skin to create a pair of elliptical wings (figures 1(*F*) and (*G*)) [10, 11]. Other lizards (genus *Ptychozoon*) use flaps of unsupported skin on the body in combination with toe and tail webbing to increase surface area, but these are less proficient gliders than most others [12, 13]. Snakes (genus *Chrysopelea*) neither create bilateral wings nor use skin as a flight surface, but instead double in width and form a concave bottom surface, creating a flattened whole-body 'wing' (figure 1(*H*)) [14–16]. Still other animals, including ants and some lizards, exhibit no obvious structural

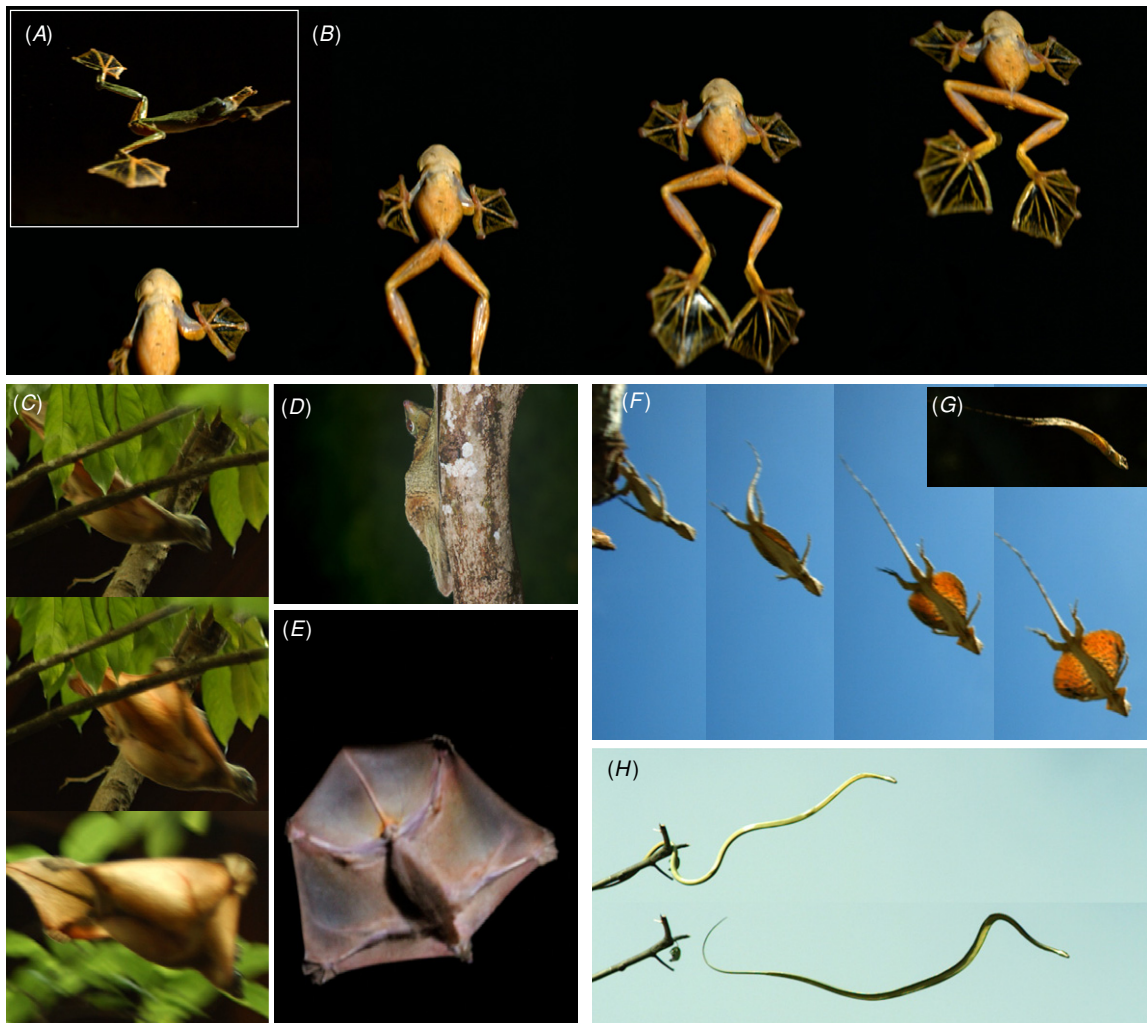[4] Author to whom any correspondence should be addressed.

Figure 1. Examples of shape and posture changes in representative terrestrial gliders. All sequences are taken from the early portion of the trajectory, in the non-equilibrium descent phase just after takeoff. (*A*) Gliding frog *Rhacophorus nigropalmatus* in side view. This posture does not represent the final glide posture; here the legs are sprawled, and as the frog moves through the initial descent it retracts its legs ((*B*), ventral view), which are fully extended after takeoff. Time interval between frames is 20 ms. (*C*)–(*E*) The colugo *Galeopterus variegatus*, a dermopteran mammal, shown in side view unfurling its patagium just after takeoff (*C*), in ventral view with patagium fully extended (*E*), and at rest gripping a tree (*D*). Time intervals between frames in (*C*) are 30 and 340 ms, sequentially. (*F*) Ventral view of a gliding lizard *Draco maculatus* shown extending its rib wings and head winglets just after taking off from a branch (left). Time interval is 38 ms. The camber of the wing can be seen in a side view in (*G*). (*H*) Dorsoventral flattening in the gliding snake *Chrysopelea paradisi*. Time interval is 225 ms. Images courtesy of National Geographic Television.

specializations but use postural adjustments to control descent [17–20].

The animal flight literature has largely focused on the steady and unsteady aerodynamics of bird, bat, and insect flight. A common element among these flyers are wings that undergo complex motions involving heaving, pitching, and feathering, and variations of acceleration between up and down strokes, resulting in time-dependent forces and moments [21]. Often these kinematics lend themselves to complex aerodynamic processes such as dynamic stall or the Weis–Fogh effect [22]. In contrast, gliding is considered the simplest form of flight [e.g. 23–25] because it appears to lack the complex three-dimensional reciprocating motions involved with flapping wings. Conceptually, gliding is often approached assuming theoretical conditions of equilibrium, in which the animal moves diagonally downward through the air with constant velocity, achieving steady horizontal travel by creating a net aerodynamic force that balances weight. Under such steady conditions, gliding performance can be easily understood and analyzed; the angle of descent, for instance, is uniquely determined by the glider's lift-to-drag ratio [25].

While this idealization of gliding flight is appealing for its tractability, in reality animal gliding is not nearly as simplistic. As noted previously (e.g. [1, 6, 24, 26]), animals can actively manipulate and modulate flight forces by changing shape, posture, or area, as when a flying squirrel or sugar glider moves its limbs to change camber and rotate the body [24, 27]. Indeed it is probable that a gliding animal will never experience perfect equilibrium during its flight, simply as a consequence of its own time-varying movements that dynamically change

its lift and drag characteristics. Continuous body adjustment may not only be possible but necessary for stability control. For example, the gliding frog *Polypedates dennysi* is slightly unstable about the yaw axis [9], and may require compensatory movements to counteract unwanted yaw torques during flight.

However, even if a terrestrial glider behaved in a strictly passive fashion while airborne, non-equilibrium dynamics must be considered because of the drastic variations inherent in the successive stages of a glider's trajectory. In contrast to active flyers (e.g. birds and insects) that can begin gliding while already fully airborne, terrestrial gliders must take off from some height and begin their trajectory in an unsteady free fall. These gliders can initiate descent from the substrate using a jump or a fall [6, 16, 28, 29], but in most cases the animal's initial velocity will be less than its equilibrium velocity, and therefore a transitional acceleration must occur. This 'accelerating descent' phase of the trajectory has received little attention, and to our knowledge there have been few attempts, if any, to predict entire glide trajectories from takeoff to equilibrium based on physical parameters alone. Overall, the potentially complicated interplay between animal behavior, unsteady kinematics, and aerodynamics suggests that animal gliding is not so simple after all.

Snakes employ by far the most dynamic gliding style of all the terrestrial gliders, and their active movements may lead to large deviations from expected equilibrium theory. To take off (from a branch), the snake drops its fore body into J-shaped loop and jumps by accelerating upward and away from the branch [16]. At the apex of the jump, the snake is relatively straight, but as it falls through a steep angle (50–60°), the body rotates in the pitch axis, the head and tail move closer forming wide body coils, and a 1–2 Hz undulation begins. This undulation is a complex 3D motion comprising side-to-side traveling waves moving from head to tail, with some evidence of body translation in the vertical axis as well. As the snake gains forward speed (reaching 8–11 m s^{-1}), it creates greater aerodynamic forces and the glide path shallows, with a descent angle on the order of 30° (but minimally as small as 13°).

Although previous studies provided these basic descriptions of snake gliding behavior [15, 30, 31], they failed to conclusively identify instances of equilibrium gliding. This lack of evidence for equilibrium may be explained in one of two ways: (1) snakes do not glide at equilibrium, possibly resulting from their active body movements or unsteady dynamics; (2) snakes can indeed achieve equilibrium given the necessary conditions, but previous experimental design has precluded proper identification. In prior studies, snakes were launched from a height of 10 m, but it is possible that these gliders require more vertical space to complete their accelerating descent phase. Furthermore, gliding kinematics were determined using three points on the snake's body, with movements tracked using two videocameras stationed above the takeoff site. As snakes glided away from the cameras, they became smaller in apparent view, resulting in increasing position error throughout the trajectory. Hence, velocity and acceleration were poorly quantified in the later stages of the glide. This large error also precluded precise determinations of

body orientation and changing posture of the snake in its fully developed glide, both of which are critical to understanding the snake's aerodynamics.

Here, we ask the following questions related to gliding flight in snakes: What are the snake's kinematics and performance in a late-phase glide, and at what point does the snake achieve equilibrium? And more generally, what are the characteristics of unsteady glide trajectory dynamics prior to equilibrium? First, we recorded gliding in snakes with improved fidelity, specifically focusing on the late stage of the trajectory. Snakes were launched from a 50% greater height than in previous studies to allow more time to develop equilibrium gliding, and an increased number of body markers and videocameras enabled a more precise determination of body posture, orientation, velocity, and acceleration. Second, we used snake characteristics to analytically model the dynamics of glide trajectories, specifically examining the effects of wing loading, lift-to-drag ratio, and takeoff velocity on unsteady trajectory characteristics. The results of these models were compared to the late-stage trajectory data to demonstrate how unsteady dynamics might lead to delayed equilibrium and oscillating forces throughout a glide. This study contributes to our understanding of the mechanics of gliding in animals and additionally provides a performance framework for the design of future bio-inspired oscillating gliders.

2. Materials and methods

2.1. Animal gliding experiments

Gliding was recorded from four 'flying' snakes (paradise tree snakes, *Chrysopelea paradisi*) wild-caught in Singapore. Snakes were housed in plastic aquaria with *ad libitum* water and branches for climbing. They were fed geckoes once per week and given two days to rest after feeding. Animal research and housing protocols were approved by the Singapore National Parks Board and the University of Chicago Animal Care and Use Committee (protocol 70963).

Glide trials were conducted outdoors in an open field in the Bukit Batok Nature Park, Singapore, in December 2003. Two scaffolding towers (heights 15 and 10 m) were constructed in the field spaced at a distance of 23 m apart (figure 2). The 15 m tower was used to launch the snakes ('launch tower'); the 10 m tower was used as a target for potential landing ('target tower') and was dressed with leafy branches at the base. The towers also served as platforms to mount four mini-DV videocameras (Sony DCR-TRV900; NTSC standard 30 interlaced fps, 720 × 480 px image size; Tokyo, Japan), with one pair on each tower. The videocameras were attached at opposing corners of the towers (spacing, 2.3 m) at heights of 10.5 m on the launch tower and 9.5 m on the target tower. The four videocameras were oriented to capture the second half of a glide trajectory, encompassing a recorded volume roughly 12 × 12 × 8 m^3. Twenty metal bolts were arranged in a grid in the ground (in view of all cameras) to serve as reference points for 3D reconstruction, and the 3D positions of the bolt heads and videocameras were measured using standard surveying
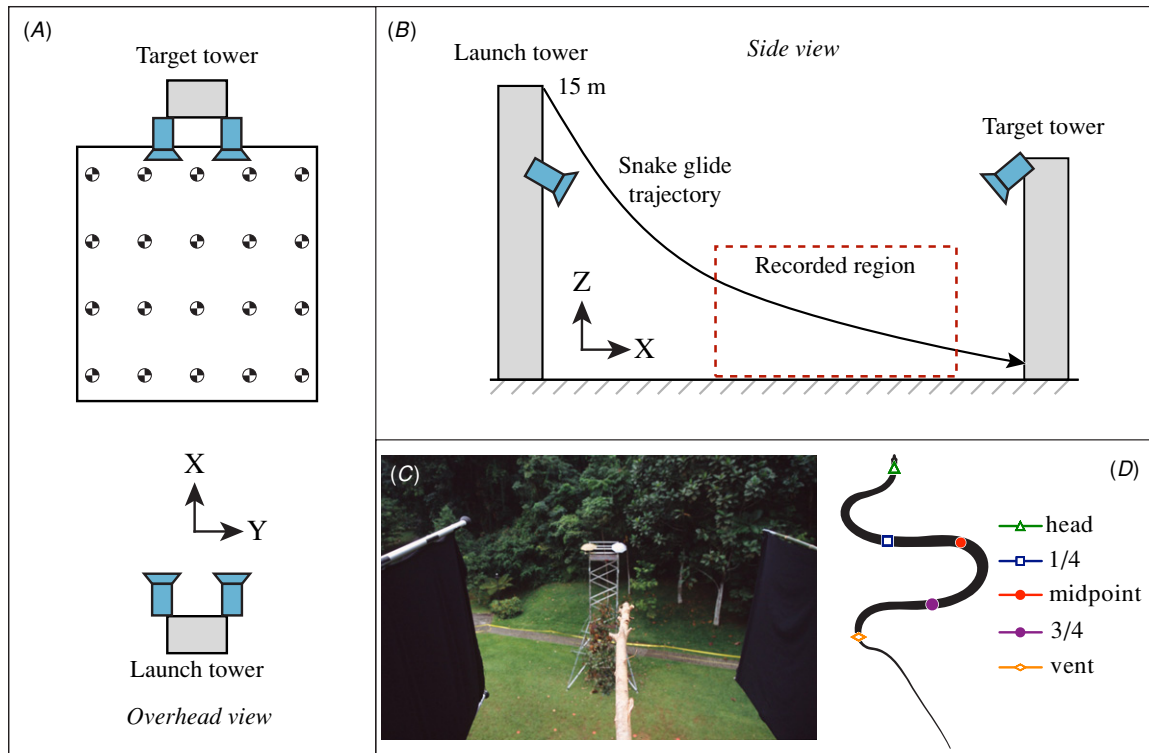
Figure 2. Experimental setup for recording snakes in late-phase gliding. (*A*) Overhead view showing placement of videocameras and ground markers used for photogrammetric reconstruction. (*B*) Side view, indicating the portion of the glide trajectory that was recorded. (*C*) Overhead view of takeoff branch, with black sheets to the side and the target tower in the distance. (*D*) Location of the five landmarks on the snake's body.

techniques. The coordinate system was defined relative to gravity, with the *x*- and *y*-axes in the horizontal plane and the *z*-axis oriented vertically; if a snake traveled straight between the towers, it moved forward along the *x*-axis and its lateral movements occurred in the *y*-axis (see figure 2). In general, the design of this experimental layout was similar to a previous system; see [31] for further details.

A tree branch (length 1.0 m, diameter 2.6 cm) mounted horizontally on the top of the launch tower ($h = 14.9$ m) was used as a takeoff substrate. Because the field site was ringed by dense forest that provided a wide array of potential landing targets for the snake, two black fabric sheets were hung vertically on each edge of the tower to restrict the snake's view and encourage glide trajectories toward the target tower (figure 2(*C*)). Despite this arrangement, some glide trials were not recorded because the snake angled its path away from the recorded glide arena.

On each day of glide trials, snakes were marked on the dorsal body with a 1 cm band of non-toxic paint (Wite-Out; Waterman-BIC, Milford, CT, USA). Five bands were painted equidistantly between the head and the vent, located as follows: just posterior to the head, one-quarter SVL, one-half SVL, three-fourths SVL, and vent (figure 2(*D*)). Prior to testing, snake length and mass were recorded.

Glide trials were conducted using a protocol similar to Socha *et al* [31] in which the snakes launched under their own volition. Snakes were brought to the top of the launch tower in a cotton reptile sack and were placed individually on the branch with the head facing toward the glide arena. Generally, snakes

crawled to the end of the branch and either immediately began the takeoff sequence, stopped and held position, or turned around and moved back toward the tower. Snakes that stopped were encouraged to launch by gentle prodding on the posterior body or tail; those that failed to launch within 10 min were removed and returned to the reptile sack. After gliding and landing, snakes were recaptured by hand, placed in the sack, and allowed to rest for at least 15 min before the next trial. For each trial, a camera flash (SB-800; Nikon, NY, USA) was pulsed within the recorded volume to serve as a video synchronization marker.

Wind speeds were negligible, measured with a digital anemometer/thermometer (Kestrel 2000; Nielsen-Kellerman, PA, USA) on the top of the launch tower. Temperature and humidity ranged from 25 to 27 °C and 84 to 93%, respectively.

2.2. Kinematics analysis

Although four animals were used, only two specimens provided consistent glide trials. Eight successful glide trials from these two snakes (mass = 25.5, 42.0 g; snout-vent length = 60.3, 74.0 cm, respectively) were analyzed fully.

Using Adobe Premiere software (version 6.0), video sequences were downloaded to a Macintosh G4 computer, synchronized, deinterlaced to yield 60 Hz images, and output as individual tiff files. To maximize visual identification of the snake and landmark points, images were level, contrast, and color adjusted using Adobe Photoshop software (version 2.0). The 3D reconstruction of the snake's five body landmark
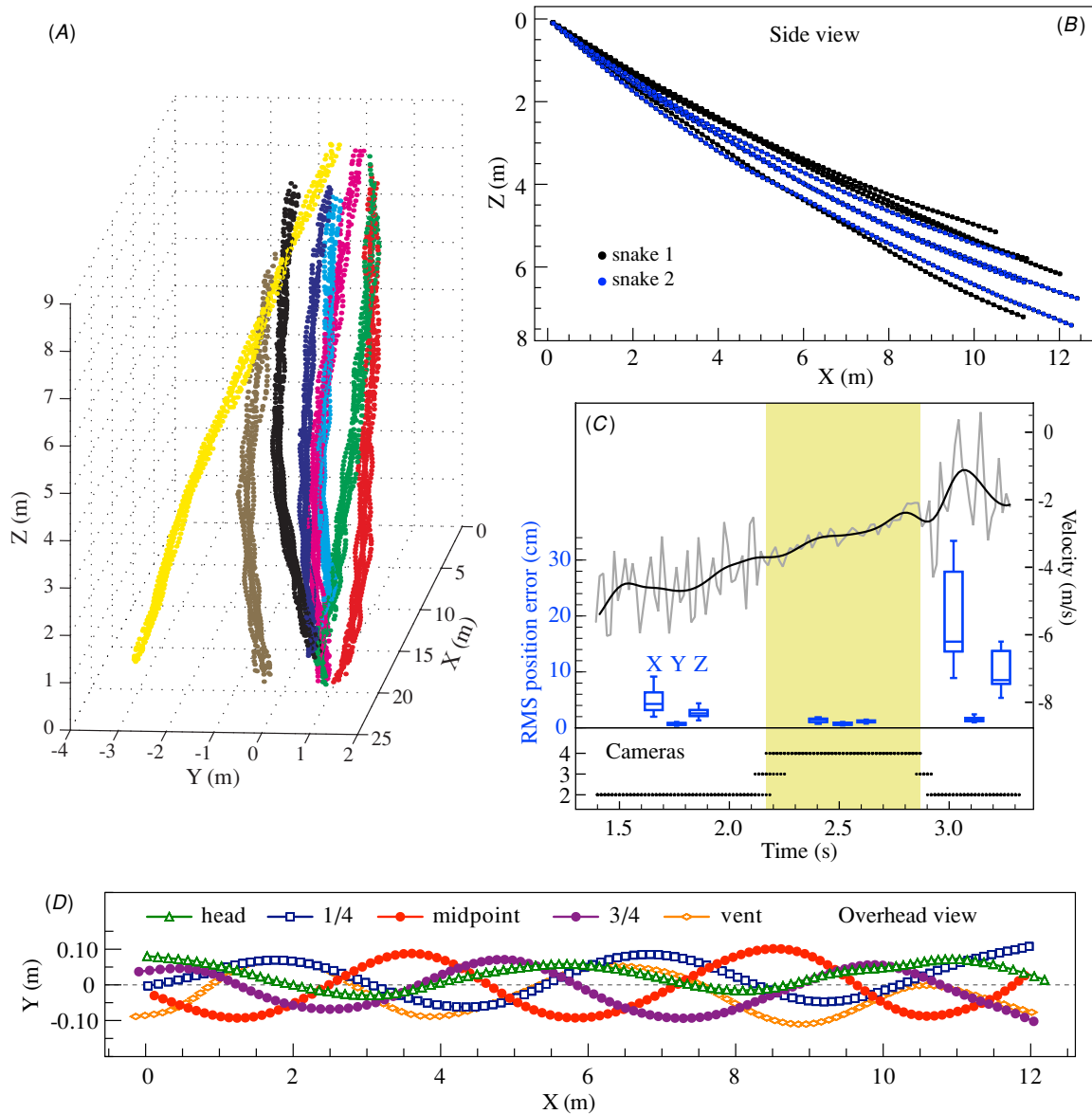
Figure 3. Snake trajectory position data. (*A*) 3D plot of raw position data from all eight trajectories, with each sequence represented in a different color. (*B*) Side view of trajectories depicting fully processed center-of-mass data, with black and blue representing the two snakes. For comparison, the origin (0, 0) has been shifted to coincide with the start of each sequence. (*C*) Position error and its effects on velocity calculation. The total average position error is shown via box plots for each axis, pooled into three regions defined by the number of cameras with the snake in view. The box plots indicate the median and first and third quartiles across all trials (*n* = 8), and whiskers represent 10% and 90% percentiles. The large differences in error in the three regions are reflected in the vertical velocity plot (gray), calculated using finite differences on the raw data. The black line depicts the velocity after filtering. (*D*) Overhead view of a trajectory showing sinusoidal movement of all five landmarks. The *Y*-axis is expanded relative to the *X*-axis to better reveal side-to-side movements; *Y* values represent displacement relative to the center of mass.

points throughout the recorded trajectory was conducted using Leica Photogrammetry Suite software (version 8.7). The RMS error of reconstructed snake coordinates, which encompasses all sources of error, varied throughout a sequence and was generally highest at the beginning and end, and smallest at mid-sequence (figure 3(*C*)). This pattern was a consequence of the arrangement of the four cameras—although their fields of view overlapped, the snake was in view of only two cameras at the beginning and end of a sequence. Specifically, average RMS error in the beginning, middle, and end of sequences was

4.9, 0.7, 2.5 cm, 1.4, 0.7, 0.9 cm, and 19.5, 1.5, 9.8 cm in the *X*-, *Y*-, and *Z*-axes, respectively.

At some instances within a glide sequence, parts of the body were obscured from view, resulting in a missing coordinate. To infer these missing points, coordinate gaps were filled using a third-order polynomial fit to four points, two before and two after the missing point within the time series.

After gap filling, the coordinate data were filtered to remove high-frequency noise. A second-order Butterworth

filter was applied, with the following equation used to determine cut-off frequency [32]:

$$f_c = \left(0.06\, f_s - 0.000\,022\, f_s^2 + 5.95\right)/\text{rms} \tag{1}$$

$$\text{rms} = \frac{\sum_i \left(x_i - x_i^f\right)^2}{\sum_i \left(x_i - \bar{x}\right)^2} \times 100 \tag{2}$$

where f_s is the sampling frequency (60 Hz), rms is the residual mean square, x_i is the raw data, $\bar{x}$ is the average, and x^f is the filtered data.

To calculate the snake's instantaneous center of mass, it is necessary to identify its time-varying body posture and mass distribution. Because our five landmark points provided an incomplete representation of body position, we attempted to estimate the whole body coordinates by spline fitting. However, initial attempts produced anatomically unreasonable results. Therefore, we chose to model the center of mass simply by assuming that the snake consisted of four segments of equal mass, with segment positions determined by the landmark coordinates using the following equation:

$$P_{\text{CoM}} = (P_{\text{head}} + 2\, P_{\text{quarter}} + 2\, P_{\text{mid}} + 2 P_{\text{three-quarter}} + P_{\text{vent}})/8 \tag{3}$$

where P is the three-dimensional position and the subscripts refer to specific landmarks.

Because the actual snake trajectories did not follow a predefined path (figure 3(A)), the coordinates were rotated to align the glide path in the *XZ* (vertical) plane. This alignment was conducted using multiple sequential rotations. First, a displacement vector was calculated using two consecutive center-of-mass coordinates. This vector was used to define the rotation angle relative to the *XZ* plane, and then all subsequent coordinates were rotated by this angle. This process was repeated sequentially throughout the trajectory, straightening the path while maintaining the total displacement of the center of mass.

After alignment in the *XZ* plane, the instantaneous velocity (v), acceleration (a), and glide angle (θ) at any time (t) were calculated as

$$v_{\text{lm}}(t) = \frac{P_{\text{lm}}(t + \Delta t) - P_{\text{lm}}(t - \Delta t)}{2\Delta t} \tag{4}$$

$$a_{\text{lm}}(t) = \frac{P_{\text{lm}}(t + \Delta t) - 2P_{\text{lm}}(t) + P_{\text{lm}}(t - \Delta t)}{\Delta t^2} \tag{5}$$

$$\theta(t) = \tan^{-1}\left(\frac{v_{\text{CoM}}^Z(t)}{v_{\text{CoM}}^X(t)}\right) \tag{6}$$

where $\Delta t = 1/60$ s is the sampling time step, and the subscript 'lm' represents any of the five body landmarks or the CoM. Also, v_{CoM}^X and v_{CoM}^Z denote the *X*- and *Z*-components of the CoM velocity.

The posture and orientation of the body were characterized by calculating relative displacements of the coordinates in each axis throughout the trajectory. Because we were interested both in body position relative to the ground and in body position relative to the oncoming airflow (relevant to aerodynamic analyses), we conducted analyses in both a gravitational reference frame and a trajectory reference frame.

For trajectory frame analyses, we first used the center-of-mass displacement vectors to sequentially rotate the local glide path into the *X*-axis (thus straightening the glide path into the horizontal axis), and then calculated displacement.

The acceleration time series resulting from this process of filtering and differentiation showed a high degree of variation, an expected result given that effects of position error are greatly magnified when accelerations are calculated as double derivatives [32]. Therefore, we additionally conducted two separate analyses on the raw, unfiltered position data to explore the effects of methodology on the acceleration results. First, we smoothed the raw data with a generalized cross-validatory quintic spline using QuickSAND software [33], and instantaneous accelerations were calculated by numerical differentiation. Second, we fit second-order polynomials to the position data and calculated acceleration as the second derivative; this produced an average acceleration over the sequence.

2.3. Theoretical modeling

To test the theoretical effects of wing loading (WL), lift-to-drag ratio (C_L/C_D), and takeoff velocity on glide performance, we conducted numerical simulations using equations of motion, assuming that only steady forces of lift, drag, and weight were acting on the body. We simulated two-dimensional glide trajectories using the following equations:

$$\text{Lift} = \tfrac{1}{2} A\rho C_L\left(v_Z^2 + v_X^2\right) \tag{7}$$

$$\text{Drag} = \tfrac{1}{2} A\rho C_D\left(v_Z^2 + v_X^2\right) \tag{8}$$

where A is the projected area, ρ is the density of air (1.2 kg m^{-3}), C_L and C_D are the lift and drag coefficients, respectively, and v is the velocity. Equations were solved numerically using the '*lsoda*' function (an ordinary differential equation solver) in the ODESolve package for the programming language R [34, 35].

Vertical and horizontal components of the aerodynamic forces were calculated and inserted into the differential equations given to the *lsoda* function to solve for the absolute vertical and horizontal accelerations (a), velocities (v), and positions (p) as a function of time (t):

$$\frac{\mathrm{d}v_X(t)}{\mathrm{d}t} = \frac{g}{2\text{WL}}\rho\left(v_Z^2(t) + v_X^2(t)\right)$$
$$\times \left(C_L \cos\left(\frac{\pi}{2} + \theta\right) + C_D \cos(\pi + \theta)\right) \tag{9}$$

$$\frac{\mathrm{d}v_Z(t)}{\mathrm{d}t} = \frac{g}{2\text{WL}}\rho\left(v_Z^2(t) + v_X^2(t)\right)$$
$$\times \left(C_L \sin\left(\frac{\pi}{2} + \theta\right) + C_D \sin(\pi + \theta)\right) - g \tag{10}$$

$$\frac{\mathrm{d}P_Z(t)}{\mathrm{d}t} = v_Z(t) \tag{11}$$

$$\frac{\mathrm{d}P_X(t)}{\mathrm{d}t} = v_X(t) \tag{12}$$

Table 1. Glide characteristics used for snake trajectory simulations. Because initial velocities were not recorded in this study, the average value reported in [31] was used for snakes 1 and 2.

Case		Wing loading (N m^{-2})	Glide angle, min (°)	Forward velocity (m s^{-1})	Initial velocity (m s^{-1})	C_L/C_D	C_L	C_D	Source
1.	Snake 1 'best'	25	18	8	1.7	3.08	0.64	0.21	This study
2.	Snake 2 'best'	29	19	8	1.7	2.90	0.74	0.25	This study
3.	Snake 1 'worst'	25	40	8	1.7	1.19	0.51	0.43	This study
4.	Snake 2 'worst'	29	42	8	1.7	1.11	0.58	0.52	This study
5.	'Best'	18	13	7	1.4	4.33	0.61	0.14	[31]
6.	'Average'	29	28	9	1.7	1.88	0.54	0.29	[31]
7.	'Worst'	46	40	10	2.5	1.19	0.60	0.51	[31]

where WL is wing loading (mg m^{-2}), g is 9.8 m s^{-2}, and ρ is the density of air (1.2 kg m^{-3}). In these simulations, g and ρ were held constant, while the values for WL, C_L, C_D, and $v_X(t = 0)$ were varied as free parameters. We used values in table 1, which were based on experimental data from this study and from Socha *et al* [31], choosing extremes of performance to define 'best', 'worst' and 'average' combinations for comparison. Additionally, we examined wing loading and C_L/C_D values beyond the snake's observed values to more fully explore the effects of these parameters.

3. Results and discussion

3.1. Trajectory dynamics

Despite being launched from a height of 15 m, neither of the two snakes tested here exhibited equilibrium gliding. In all eight trials, velocity and glide angle changed continuously throughout each sequence (figure 4(A)). Forward velocity began around 8 m s^{-1} and decreased slightly, while the vertical speed decreased from ∼6 to ∼4 m s^{-1}. Concomitantly, glide angle decreased from 32–42° to 18–23° at a rate of $-10 \pm 2°$ s^{-1}. These changes in vertical speed and glide angle are reflected in the vertical acceleration data, which reveal a positive (upward) acceleration. Across the entire recorded sequence, the second-order polynomial fitting shows an average vertical acceleration of 1.8 ± 0.5 m s^{-2} (mean ± SD, $n = 8$). Instantaneous data from the four-camera region, which produced the lowest spatial error and therefore the most reliable data, show an average acceleration of 1.5 ± 0.7 m s^{-2} ($n = 8$) and 1.4 ± 0.7 m s^{-2} ($n = 8$), calculated from the filtered and spline fit data, respectively. Undulation frequencies were consistent among trials, with snakes moving from side-to-side at a frequency of 2.0 ± 0.2 Hz ($n = 8$).

The trajectory simulations revealed damped oscillations in acceleration that produced variations in velocity and glide angle (figures 5 and 6). Accelerations in the horizontal and vertical axes began with an initial increase, with the peak in a_z always lagging the peak in a_x. In general, oscillations were damped with a corresponding time scale of seconds. These simulations suggest that it is theoretically possible for a glider to have a positive acceleration in the vertical axis without any active modulation by the animal itself; passive trajectory dynamics alone are sufficient to create a net upward force.
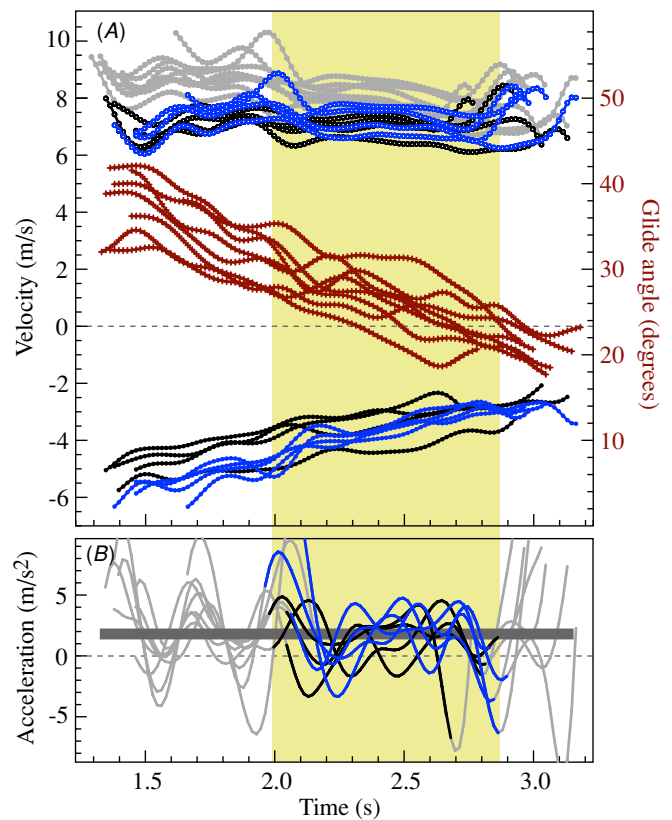

Figure 4. Glide sequence summaries. The region of four camera overlap (with lowest position error) is shown in yellow, as in figure 3(C). (A) Velocity and glide angle through time for each trial. Overall velocity is in gray; v_x and v_z are represented with circles and crosses, respectively, and glide angle is in red. Black and blue lines represent the two snakes. (B) Vertical acceleration for each trial. The traces represent the instantaneous acceleration values calculated from the filtered data. The grayed portions of the traces indicate regions of higher variance, which likely originates from the relatively greater position error of these regions. Also shown is the average acceleration pooled across all eight trials (straight gray line, $a = 1.8$ m s^{-2}), calculated using a second-order polynomial; the line thickness represents one standard deviation about the mean. In all graphs, the time prior to the start of the sequence from the start of the trajectory (1.33 ± 0.15 s, $n = 6$) was estimated using data from a previous study [31] using similar-sized snakes.

Viewed broadly, the simulations produced qualitatively similar results compared to the experimental data. Because actual C_L and C_D were not known, we framed our initial
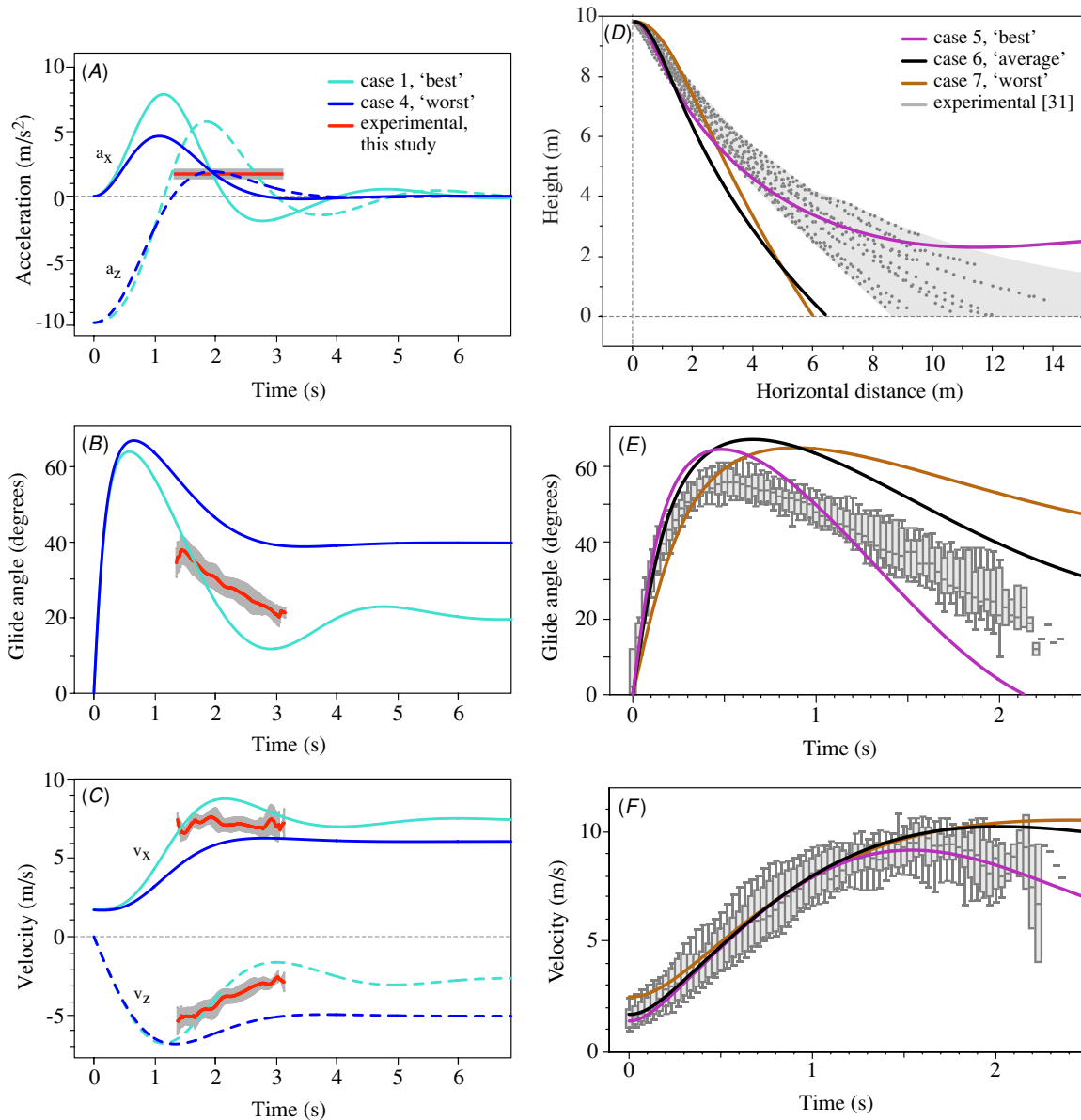
Figure 5. Comparison of simulated and experimental snake glides. Model input values are given in table 1. (*A*)–(*C*) Acceleration, glide angle, and velocity in cases 1 (light blue) and 4 (dark blue) versus pooled experimental data from this study (red). The gray bands represent the range of values for each trial (*n* = 8). For (*A*), the red line represents the average acceleration across the entire trial, calculated using a second-order polynomial fit to the velocity data. The simulations for snake 1 and 2 were indistinguishable, and therefore only one case from each is shown. (*D*)–(*E*) Position, glide angle, and velocity in cases 5 (purple), 6 (black), and 7 (brown) versus experimental data from a previous study [31] (gray), examining trajectories from *t* = 0. Experimental data represent trials from 14 snakes of the same species (*Chrysopelea paradisi*) used in this study; the box plots indicate the mean and first and third quartiles, and whiskers represent 10% and 90% percentiles.

conditions based on extremes of observed glide angles at the beginning ($\theta = 42°$) and end ($\theta = 18°$) of the sequence, which correspond to lift-to-drag ratios of 3.08 and 1.11, respectively (table 1). These two simulations bounded the experimental data (figures 5(*A*)–(*C*)), with the $C_L/C_D = 3.08$ simulation most closely matching experimental glide angles and velocities (figure 5(*B*)), and the $C_L/C_D = 1.11$ simulation more similar in acceleration in the vertical axis (figure 5(*A*)). However, there were differences in fine-scale details. Although the model accurately predicted the glide angle at the beginning of the sequence with $C_L/C_D = 3.08$, the experimental glide angles

decreased at a slower rate in direct comparison, meaning that the trajectories of the real snakes shallowed more gently. This difference is reflected in the vertical velocity (figure 5(*C*)), where the experimental values also decreased more slowly for $C_L/C_D = 3.08$ but was similar for $C_L/C_D = 1.11$. Lastly, the model predicted a positive, varying vertical acceleration from 1 to 3 s, and the experimental data also reveal a positive acceleration during that time (figure 5(*A*)). Figure 5(*A*) compares the model only to the average acceleration calculated with the second-order polynomial; close comparison with the time-varying acceleration data should be viewed with
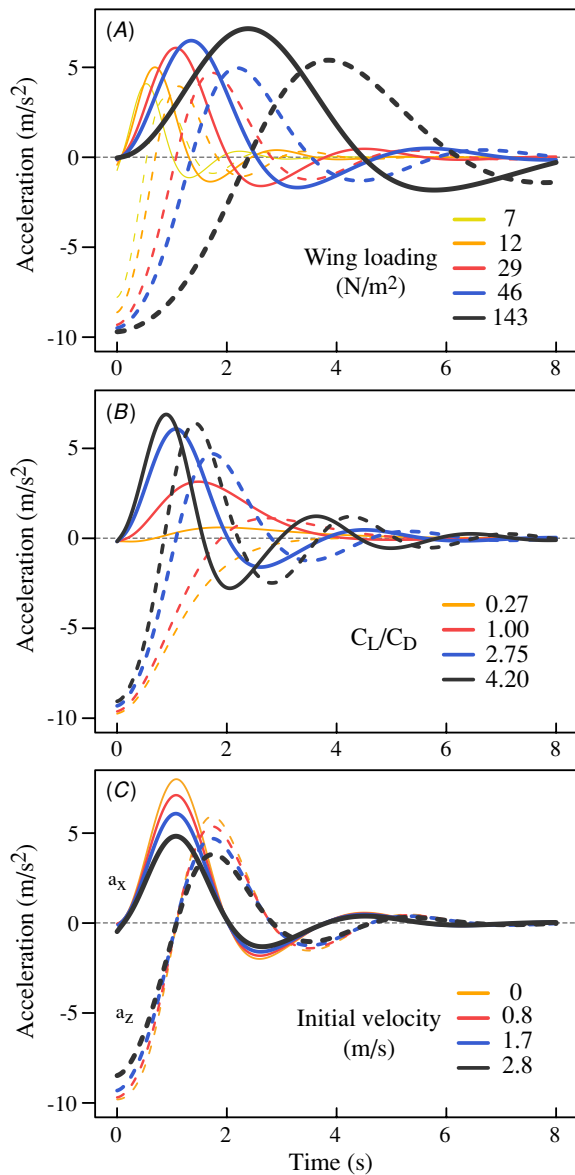
Figure 6. Theoretical effects of wing loading (*A*), lift-to-drag ratio (*B*), and initial horizontal velocity (*C*) on acceleration in simulated snake glides. Each parameter was varied independently, using the base condition as WL = 29 N m^{-2}, C_L/C_D = 2.75 (equivalent to $\theta = 20°$ in equilibrium), and v_{initial} = 1.7 m s^{-1}. Horizontal and vertical values are depicted with solid and dashed lines, respectively.

caution due to the high error inherent in second derivatives used to calculate acceleration [32]. Better time-accurate acceleration information could be obtained in future studies using accelerometers attached to the snake's body (e.g. [6]). At the time when the experiment was conducted, accelerometer systems that were sufficiently small (~1 g, self-contained) were not available, but this approach is now becoming possible.

When compared to previous experimental data that detailed the earliest portion of the trajectory (from $t = 0$ to ~2 s) [31], the model performed similarly (figures 5(*D*)–(*F*)), bounding the real data but proving inadequate for all details. In particular, the simulated glide paths were markedly different than those of the real snakes. Both the 'average'

and 'worst' cases provided trajectories that were more steep than the experimental, resulting in lower horizontal distance traveled (figure 5(*D*)). This difference was reflected in the glide angle data (figure 5(*E*)), with the model predicting a greater maximum glide angle in the accelerating descent phase and a greater time to transition to trajectory shallowing. However, actual shallowing rates were similar. For the 'best' case, the model indicated a greater maximum glide angle and greater shallowing rate, which produced a path that was more curved (including an upward incline at the end) than was observed in the experimental data. Despite these differences, the model produced similar velocities for all cases (figure 5(*F*)).

Overall, comparisons between simulated and real trajectories indicate that a more sophisticated model is required to fully capture the features of snake gliding flight. Throughout the trajectory, the undulating gliding snake undergoes large changes in body posture, orientation, and speed, suggesting that lift and drag coefficients are time-varying, contrasting with the steady-state assumption of our simple model. For example, angle of attack likely varies throughout a trajectory, but there are currently no high-fidelity data on angle of attack in gliding snakes, and in general for most vertebrate gliders (however, see [24, 27, 36]). Another consideration is that the snake may be using unsteady lift generating mechanisms, which would require additional refinements to the model. To address these issues, it would be beneficial to measure actual forces and quantify flows on the airborne animal and/or to test physical and computational models, work that we are currently undertaking and developing.

3.2. Implications of theoretical modeling

Although the theoretical model used here is not adequate to precisely predict snake trajectory dynamics, it provides a first-order physical representation of its gliding aerodynamics, and therefore can be used to make general quantitative predictions about the effects of wing loading, lift-to-drag ratio, and takeoff velocity. Using information from the snakes in this study as a reference, we explored the effects of varying these parameters independently. To compare between simulations, we defined the time to equilibrium (t_{eq}) as the first point for which glide angle (θ) remained within 5% of its asymptotic value:

$$0.95 * \theta_{\text{eq}} \leqslant \theta(t_{\text{eq}} \leqslant t < \infty) \leqslant 1.05 * \theta_{\text{eq}}. \qquad (13)$$

The simulations show that, as wing loading increased, the magnitude of acceleration oscillations increased and the frequency decreased, resulting in a greater time to equilibrium (figure 6(*A*)). Although this result is not surprising, our model provides the first quantitative predictions for the time it takes a glider to reach equilibrium. For snakes (WL = 12–46), t_{eq} is on the order of 3.3–6.6 s and requires a vertical travel of 6.5–26.5 m. These values suggest that equilibrium gliding may occur in the snake's native Southeast Asian forest habitat. However, little is known about the ecology of gliding in snakes; typical takeoff heights and glide distances are of particular interest but are currently unreported. Reducing wing loading to 7 N m^{-2}, the minimum literature value for *Draco* lizards [37], decreased t_{eq} to 2.5 s. Indeed, McGuire and Dudley [37] reported that 48% of their experimentally recorded *Draco*
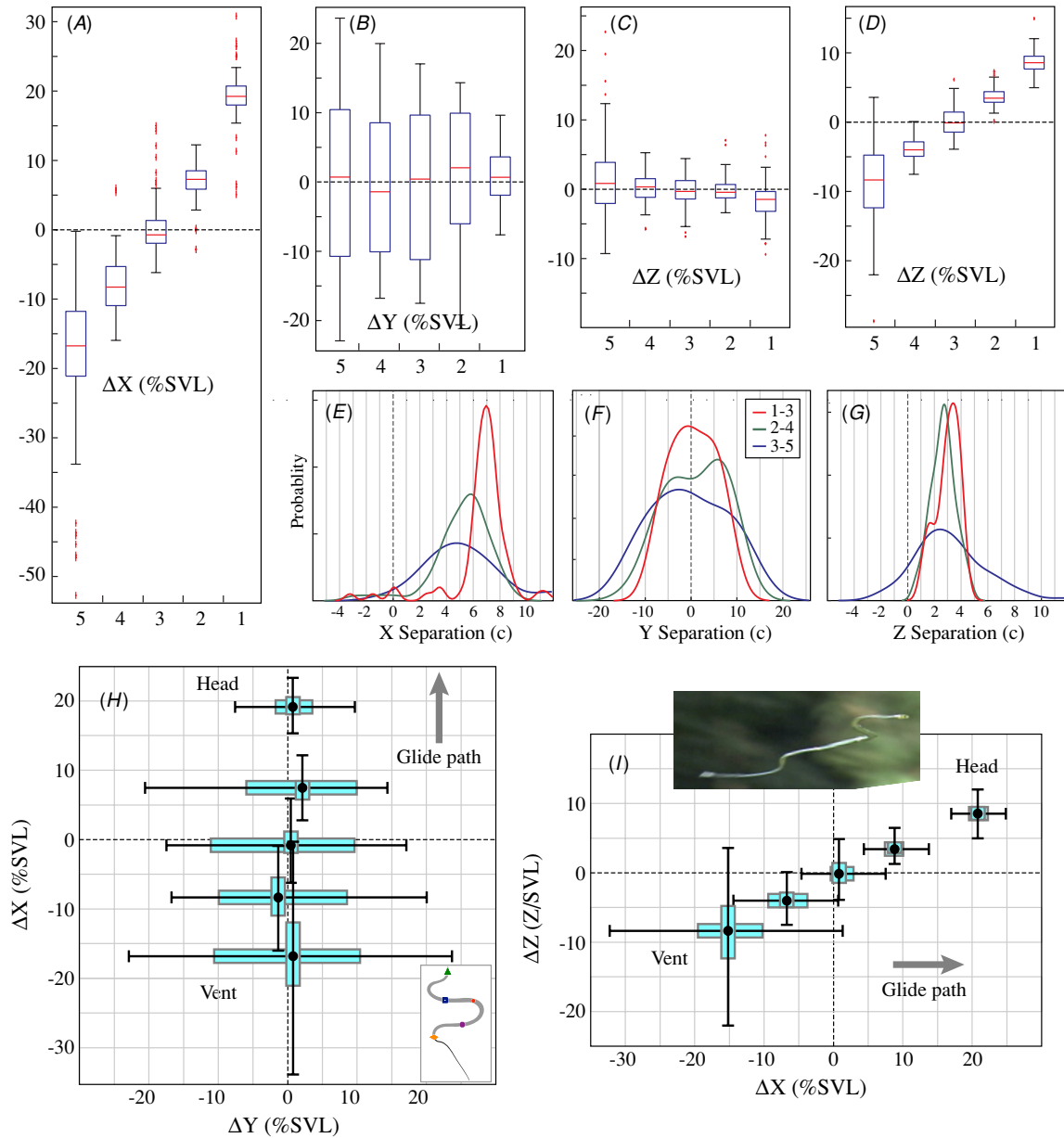
Figure 7. Summary of body posture during late-phase gliding in *C. paradisi*. All graphs except (*C*) represent values calculated in the trajectory reference frame. The box plots indicate the mean and first and third quartiles, with whiskers representing 10% and 90% percentiles and red dots outliers. (*A*)–(*D*) Box plots summarizing displacements of the five landmarks (1–5; head-vent; respectively) relative to the center of mass. For comparison, displacements are shown in percent body length (%SVL). (*C*) *Z* displacement in the gravitational reference frame, showing the body oriented relatively parallel to the horizontal. Relative to the glide path (*D*), the body is held in a staggered configuration with each downstream body segment vertically lower than the upstream segment. (*E*)–(*G*) Separation of the body segments in units of chords, calculated using displacements from points 1–3, 2–4, and 3–5. (*H*), (*I*) Summary of displacements in overhead and side views, normalized by SVL.

glides included an equilibrium component, and further showed that wing loading was negatively correlated with equilibrium gliding. For lizards with wing loading less than 10 N m^{-2}, 74% of their trials included equilibrium gliding. In our model, increasing WL to 143 N m^{-2}, the maximum reported for flying squirrels [38], increased t_{eq} to 11.7 s. Given that trajectory durations in the wild occur on the scale of seconds, these times can represent a large fraction of a total glide. For example, in a large study of 222 colugo glides in the wild [6], trajectory duration ranged from 0.6 to 15 s and averaged 3.5 s, indicating

that natural glides are typically complete within seconds. Clearly, this analysis suggests that the non-equilibrium flight may dominate real glide trajectories, particularly for animals with higher wing loadings.

When the lift-to-drag ratio was varied, the trend was different from that of wing loading (figure 6(*B*)). In these simulations, we varied the ratio by holding C_D constant and varying C_L. Increasing the lift-to-drag ratio resulted in greater frequency and magnitude of accelerations, but the accelerations were less damped, which led to a greater time

to equilibrium. Thus, there is a trade-off: achieving greater horizontal distance via increased C_L/C_D requires a greater non-equilibrium component of the glide trajectory, including more intense oscillations and therefore more complicated stability requirements. More broadly, gliders such as ants, with steep angles of descent and low L/D ratios [18, 19], likely experience far more equilibrium gliding than do gliders with shallow glide paths and larger L/D.

In contrast, varying initial velocity had comparatively minor effects on simulated glides (figure 6(C)). As initial horizontal velocity increased, the amplitude of acceleration oscillations decreased, which shows that a glider's takeoff may serve to reduce force variations early in the trajectory and therefore may have stability implications. However, this effect did not change the frequency of oscillation, and the time to equilibrium was unaffected. Although this suggests that effects of takeoff velocity are minor when considering equilibrium timing in long trajectories, initial velocity should be relatively more important for shorter glides, for which the distance gained may determine whether a landing target is successfully reached. Lastly, takeoff velocity can be relevant for non-trajectory reasons, such as quick escape from predators or interactions between males.

3.3. Snake body orientation

The experimental data presented here provide the first details of snake body orientation in a fully developed glide, summarized in figure 7. Consistent with previous data [31], the largest movements of the body occurred in the lateral (*Y*) axis, with the head exhibiting less than twice the excursion as the other landmark points (figure 7(B)). Along the forward (*X*) axis, the body maintained a staggered configuration; here the first four landmarks moved roughly equal relative distances, while the vent traveled a ∼3X greater distance. In the vertical (*Z*) axis, the body was generally oriented level with the ground when considered in the gravitational reference frame (figure 7(C)). Similar to the pattern in the forward axis, the first four landmarks moved with equal excursion, but excursion of the vent was twice great, with equal travel above and below the center of mass. When viewed in the flow-relevant trajectory reference frame, on average the snake held its body in a vertically staggered configuration with the head highest and vent lowest, forming an average body angle of 25° from the glide path. Because the airborne snake's twist about its long axis is not known, the exact angle of attack along the body cannot be determined from these data. However, if one assumes that the ventral surface of the snake faces downward, this body orientation implies angles of attack around 25°. A previous modeling study [14] indicated that flying snake-like cross-sections experience maximum lift at an angle of attack of 30°; together, these data suggest that snakes in a fully developed glide orient the body in a posture that optimizes lift production.

The results from the orientation and posture analysis provide a basis for speculation on the aerodynamic mechanism that underlies the snake's unusual gliding behavior and performance. In general, any flexible body that interacts with the incident flow will experience a fluid-structure-interaction (FSI), whereby flow-induced loads will induce a response of the body, which in turn will transfer momentum to the flow [39]. Because the snake's half-cylinder-like cross-section more closely resembles a bluff body than a streamlined airfoil, its FSI may induce a vortex-streak similar to the wake of circular cylinders, which 'lock-on' to a characteristic frequency [40]. The increasing amplitude of undulation away from the head, as well as the distinct range of body segment spacings shown in figures 7(E)–(G), suggests that the snake may be actively tuning its body undulation to a characteristic frequency. If so, it is possible that the gliding snake generates vortex-induced lift.

Moreover, the previous modeling study [14] suggests that the snake's unconventional cross-sectional shape allows the snake to delay stall for angles of attack on the order of 30°. Maintaining lift at such high angles of attack is often indicative of dynamic-stall processes and unsteady flow [22]. This suggests that the snake exploits another potential vortex-induced lift mechanism which could be effective under quasi-steady or unsteady conditions. However, this prior study used a rough approximation of body shape [14], and a high-fidelity investigation of the aerodynamics of the true anatomical shape is still needed to test these hypotheses. Finally, the role of transverse body undulations on the laminar flow along the body remains unknown. These oscillations will generate vorticity and boundary layer structures along the body; determining how these interactions specifically affect the flow and separation around the snake will require future investigations. Because a biomimetic undulating flying snake device has not yet been developed, this work will involve challenging simulations and flow visualization experiments with live animals. Overall, the favorable aerodynamic characteristics of the snake's cross-sectional shape [14] and the potential advantages of the gliding posture and kinematics for exploiting induced FSI's may provide inspiration for unconventional concepts for improving the performance of small, low Reynolds number air vehicles.

Acknowledgments

References

[1] Dudley R, Byrnes G, Yanoviak S P, Borrell B, Brown R M and McGuire J A 2007 Gliding and the functional origins of flight: biomechanical novelty or necessity? *Annu. Rev. Ecol. Evol. Syst.* **38** 179–201

[2] Breder C M 1929 Field observations on flying fishes; a suggestion of methods *Zoologica* **9** 295–312

[3] Davenport J 1994 How and why do flying fish fly? *Rev. Fish Biol. Fish.* **4** 184–214

[4] Macia S, Robinson M P, Craze P, Dalton R and Thomas J D 2004 New observations on airborne jet propulsion (flight) in squid, with a review of previous reports *J. Mollus. Stud.* **70** 297–99

[5] Bishop K L 2008 The evolution of flight in bats: narrowing the field of plausible hypotheses *Q. Rev. Biol.* **83** 153–69

[6] Byrnes G, Lim N T L and Spence A J 2008 Take-off and landing kinetics of a free-ranging gliding mammal, the Malayan colugo (*Galeopterus variegatus*) *Proc. R. Soc. B: Biol. Sci.* **275** 1007–13

[7] Thorington R W and Heaney L R 1981 Body proportions and gliding adaptations of flying squirrels (*Petauristinae*) *J. Mammal.* **62** 101–14

[8] Emerson S B and Koehl M A R 1990 The interaction of behavioral and morphological change in the evolution of a novel locomotor type: 'flying' frogs *Evolution* **44** 1931–46

[9] McCay M G 2001 Aerodynamic stability and maneuverability of the gliding frog *Polypedates dennysi J. Exp. Biol.* **204** 2817–26

[10] McGuire J A 2003 Allometric prediction of locomotor performance: an example from southeast Asian flying lizards *Am. Nat.* **161** 337–49

[11] Russell A P and Dijkstra L D 2001 Patagial morphology of Draco volans (Reptilia: Agamidae) and the origina of glissant locomotion in flying dragons *J. Zool.* **253** 457–71

[12] Russell A P, Dijkstra L D and Powell G L 2001 Structural characteristics of the patagium of Ptychozoon kulhi (Reptilia: Gekkonidae) in relation to parachuting locomotion *J. Morphol.* **247** 252–63

[13] Young B A, Lee C E and Daley K M 2002 On a flap and a foot: aerial locomotion in the 'flying' gecko, *Pychozoon kuhli J. Herpetol.* **36** 412–8

[14] Miklasz K, LaBarbera M, Chen X and Socha J J 2010 Effects of body cross-sectional shape on flying snake aerodynamics *Exp. Mech.* **50** at press

[15] Socha J J 2002 Gliding flight in the paradise tree snake *Nature* **418** 603–4

[16] Socha J J 2006 Becoming airborne without legs: the kinematics of take-off in a flying snake, *Chrysopelea paradisi J. Exp. Biol.* **209** 3358–69

[17] Jusufi A, Goldman D I, Revzen S and Full R J 2008 Active tails enhance arboreal acrobatics in geckos *Proc. Natl. Acad. Sci.* **105** 4215–9

[18] Yanoviak S, Fisher B and Alonso A 2008 Directed aerial descent behavior in African canopy ants (Hymenoptera: Formicidae) *J. Insect Behav.* **21** 164–71

[19] Yanoviak S P, Dudley R and Kaspari M 2005 Directed aerial descent in canopy ants *Nature* **433** 624–6

[20] Yanoviak S P, Munk Y, Kaspari M and Dudley R 2010 Aerial manoeuvrability in wingless gliding ants (*Cephalotes atratus*) *Proc. R. Soc. B: Biol. Sci.* **277** 2199–204

[21] Maxworthy T 1981 The fluid-dynamics of insect flight *Annu. Rev. Fluid Mech.* **13** 329–50

[22] Dickinson M H 1996 Unsteady mechanisms of force generation in aquatic and aerial locomotion *Am. Zool.* **36** 537–54

[23] Biewener A A 2003 *Animal Locomotion* (New York: Oxford University Press) p 296

[24] Bishop K L 2006 The relationship between 3-D kinematics and gliding performance in the southern flying squirrel, *Glaucomys volans J. Exp. Biol.* **209** 689–701

[25] Vogel S 1994 *Life in Moving Fluids* 2nd edn (Princeton: Princeton University Press) p 467

[26] Wakeling J M and Ellington C P 1997 Dragonfly flight: I. Gliding flight and steady-state aerodynamic forces *J. Exp. Biol.* **200** 543–56

[27] Bishop K L 2007 Aerodynamic force generation, performance and control of body orientation during gliding in sugar gliders (*Petaurus breviceps*) *J. Exp. Biol.* **210** 2593–606

[28] Essner R L 2002 Three-dimensional launch kinematics in leaping, parachuting and gliding squirrels *J. Exp. Biol.* **205** 2469–77

[29] Paskins K E, Bowyer A, Megill W M and Scheibe J S 2007 Take-off and landing forces and the evolution of controlled gliding in northern flying squirrels *Glaucomys sabrinus J. Exp. Biol.* **210** 1413–23

[30] Socha J J and LaBarbera M 2005 Effects of size and behavior on aerial performance of two species of flying snakes (*Chrysopelea*) *J. Exp. Biol.* **208** 1835–47

[31] Socha J J, O'Dempsey T and LaBarbera M 2005 A 3-D kinematic analysis of gliding in a flying snake, *Chrysopelea paradisi J. Exp. Biol.* **208** 1817–33

[32] Winter D A 2009 *Biomechanics and Motor Control of Human Movement* 4th edn (Hoboken, NJ: Wiley) p 370

[33] Walker J A 1998 Estimating velocities and accelerations of animal locomotion: a simulation experiment comparing numerical differentiation algorithms *J. Exp. Biol.* **201** 981–95

[34] Hindmarsh A C 1983 ODEPACK, A systematized collection of ODE solvers *Scientific Computing* ed R W Stepleman (Amsterdam: North-Holland) pp 55–64

[35] Petzold L R 1983 Automatic selection of methods for solving stiff and nonstiff systems of ordinary differential equations *SIAM J. Sci. Stat. Comput.* **4** 136–48

[36] Bishop K L and Brim-DeForest W 2008 Kinematics of turning maneuvers in the southern flying squirrel, *Glaucomys volans J. Exp. Zool.* A **309** 225–42

[37] McGuire J A and Dudley R 2005 The cost of living large: comparative gliding performance in flying lizards (Agamidae: Draco) *Am. Nat.* **166** 93–106

[38] Stafford B J, Thorington R W and Kawamichi T 2002 Gliding behavior of Japanese giant flying squirrels (*Petaurista leucogenys*) *J. Mammal.* **83** 553–62

[39] Paidoussis M P 1998 *Fluid-Structure Interactions: Vol 1. Slender Structures and Axial Flow* (San Diego, CA: Academic) p 572

[40] Williamson C H K and Roshko A 1988 Vortex formation in the wake of an oscillating cylinder *J. Fluid Struct.* **2** 355–81